PERGAMON

Journal of Structural Geology 24 (2002) 1491–1505

JOURNAL OF STRUCTURAL GEOLOGY

www.elsevier.com/locate/jstrugeo

Sillimanite-bearing shear zones in syntectonic leucogranite: fluid-assisted brittle–ductile deformation under amphibolite facies conditions

Giovanni Musumeci*

Dipartimento Scienze della Terra, Via S. Maria 53, 56126 Pisa, Italy

Received 24 May 2000; revised 30 August 2001; accepted 30 October 2001

Abstract

In the Imja Kola valley (eastern Nepal), Miocene peraluminous leucogranite dykes were emplaced within transtensional shear zones synchronously with regional amphibolite–facies metamorphism in the metamorphic host rocks. Within the dykes the magmatic foliations, parallel to the metamorphic schistosity, are cross-cut by thin (millimetre to centimetre size) shear zones, which are made up of prismatic and/or fibrolitic sillimanite with a minor amount of white mica. These structures have a heterogeneous distribution and form networks of strongly deformed and foliated layers wrapping around poorly deformed granitic pods. The textural and strain features are consistent with development of sillimanite shear zones as a result of heterogeneous deformation and fluid action, which allowed the replacement of strained magmatic minerals such as feldspar and biotite by means of incongruent pressure solution. The described example illustrates that nucleation and development of heterogeneous shear zones under amphibolite facies conditions, is also strongly favoured by brittle fracturing and fluid action at the grain-scale along pre-existing planes of weakness. The growth of cracks and fractures can be regarded as a sequence of short lived brittle events, due to work hardening, which punctuate a history of plastic deformation.

Keywords: Sillimanite-bearing shear zones; Syntectonic leucogranite; Granitic pods

1. Introduction

Fluid-assisted deformation and metamorphic reactions within shear zones locally result in the development of more ductile mineral assemblages, which facilitate a preferential partitioning of the strain. This process leads to the development of strongly deformed layers within a less deformed or undeformed rock. A clear relationship can be recognised between the degree of strain registered in the shear zones and the growth of new mineral assemblages by replacement reactions (Brodie and Rutter, 1985). As stated by Wintsch (1985), the applied deformation exerts a strong influence by affecting the kinetics of mineral reactions in several ways such as: (1) stored strain; (2) grain size reduction; (3) shear heating; (4) stress gradient. All these factors imply that mechanical energy is transformed into chemical energy, allowing the reaction of deformed grains and their replacement by new mineral assemblages. Moreover, the occurrence of a syndeformational fluid phase enhances the development of replacement reactions because it allows dissolution of reactant minerals, leaching and precipitation of product minerals in dilatant fractures. Such processes are well understood in retrograde shear zones; indeed pressure solution and/or incongruent pressure solution are regarded as one of the most effective deformation mechanisms under greenschist and amphibolite facies conditions (Beach, 1979; Bell and Cuff, 1989; McCaig, 1987).

This paper describes sillimanite-bearing small-scale shear zones (centimetre to decimetre widths) in synextensional peraluminous leucogranites in the Higher Himalayan Crystallines (south of Mt. Everest). The nucleation and growth of these shear zones due to incongruent pressure solution under amphibolite facies conditions is described and the development of heterogeneous brittle–ductile shear zones under amphibolite facies conditions is addressed.

2. Geology of the Khumbu region

The geology of the Khumbu region, south of Mt. Everest (eastern Nepal; Fig. 1), is dominated by the Higher Himalayan Crystallines (HHC; Carosi et al., 1999 and references therein), which represents a complex of medium- and high-grade metamorphic rocks, bounded to the south by

* Tel.: +39-50-847111; fax: +39-50-500932.
E-mail address: gm@dst.unipi.it (G. Musumeci).

0191-8141/02/$ - see front matter
PII: S0191-8141(01)00153-5

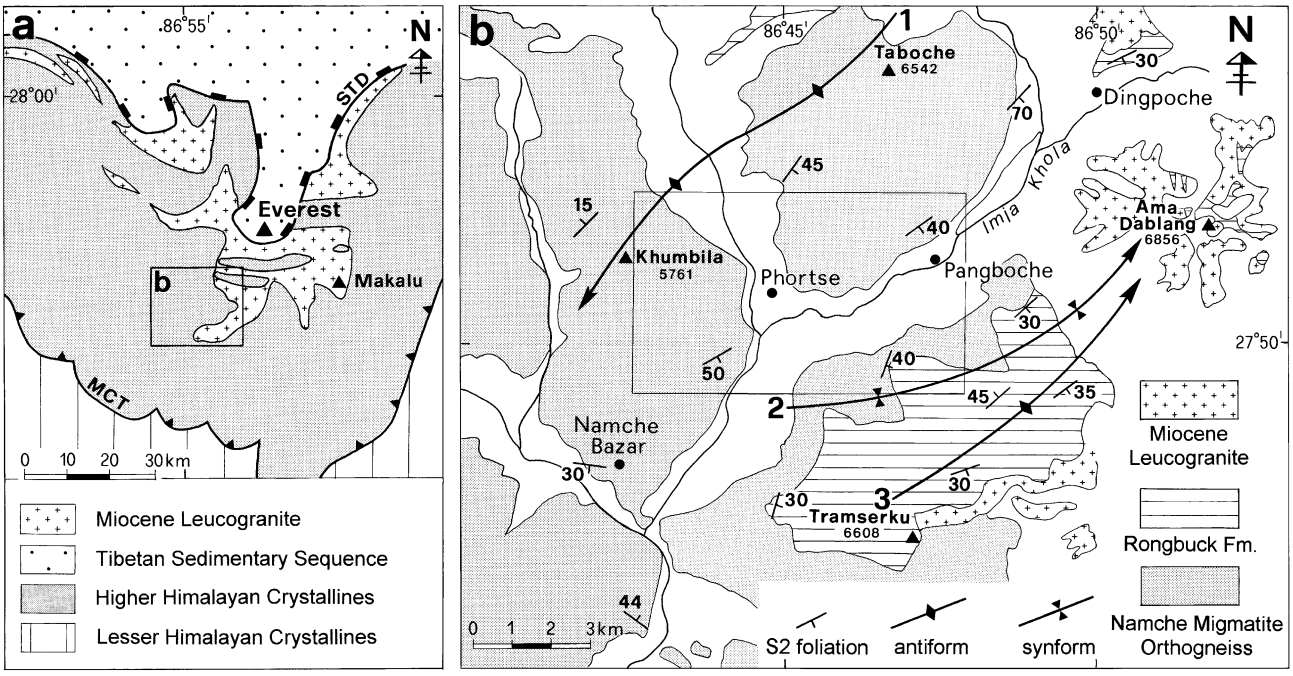

Fig. 1. (a) Geological map of Himalayan belt in eastern Nepal. STD: Southern Tibetan Detachment; MCT: Main Central Thrust. (b) Structural sketch map of the Imja Kola valley (after Carosi et al., 1999). 1: Taboche Antiform, 2: Ama Dablang Synform, 3: Tramserku Antiform. The inset shows the area in Fig. 2.

the Main Central Thrust (MCT; Bordet, 1977; Brunel, 1983) and to the north by the South Tibetan Detachment System (STDS; Burg et al., 1984). The latter is a gently northward dipping Lower Miocene ductile extensional fault system, which juxtaposes unmetamorphosed sedimentary rocks of the Tibetan Sedimentary Sequence onto high grade metamorphic rocks of the HHC (Burchfiel et al., 1992; Carosi et al., 1998).

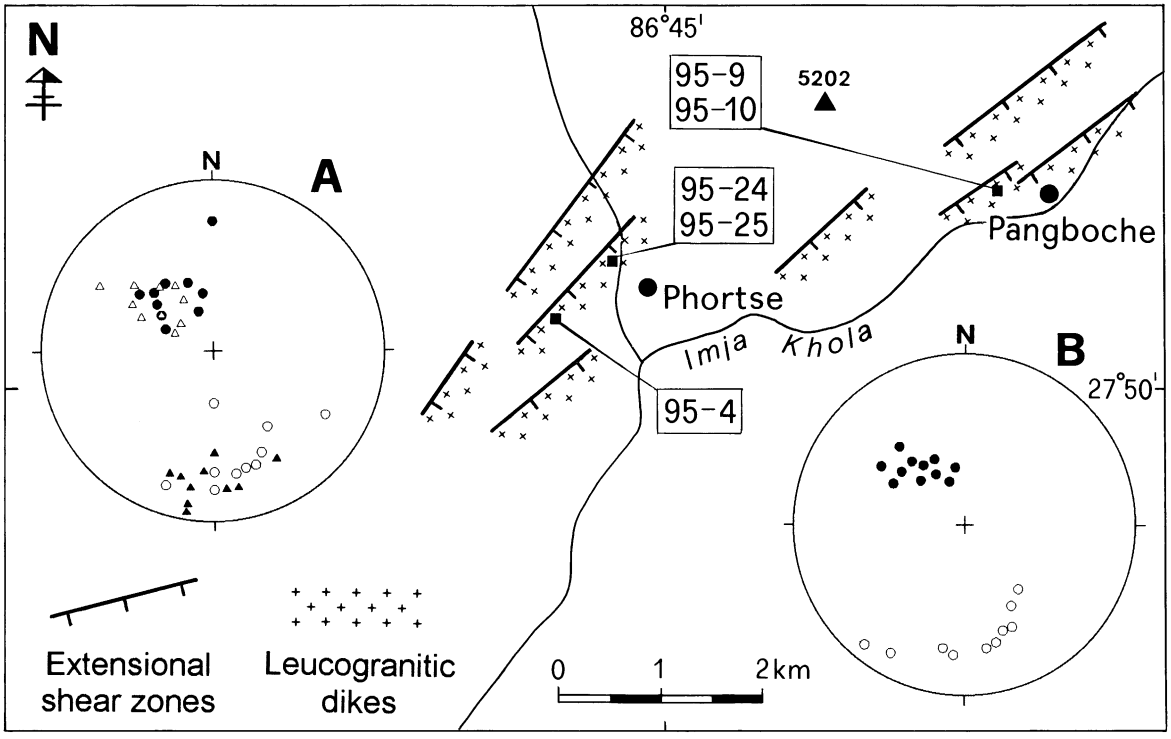

Fig. 2. Distribution of extensional faults and systems of synkinematic leucogranite dykes in the Imja Kola valley and sample locations. (a) and (b) Lower hemisphere equal area stereographic plots. (A) Poles to extensional fault zones (filled circles), slickenside lineations on fault planes (open circles), poles to magmatic foliations (open triangles), magmatic lineations (filled triangles). (B) Poles to sillimanite layers (filled circles), mineral lineations (open circles).

In the Khumbu region (Fig. 1b) the HHC is made up of a sequence of upper amphibolite facies gneiss and granitic orthogneiss (Barum Gneiss and Namche Migmatite Orthogneiss), overlain by biotite and sillimanite-bearing paragneiss and micaschists (Black Gneiss). At the top of the sequence, biotite and muscovite-bearing gneiss (Rongbuck Formation) crops out, immediately below the South Tibetan Detachment. Metamorphic grade decreases upwards across this sequence and within the HHC a polyphase metamorphic evolution has been recognised (Lombardo et al., 1993); an early Himalayan event of Barrovian type, (only recorded in the Barum Gneiss and Rongbuck Formation), was followed by a late Himalayan high temperature–low pressure event reflecting nearly isothermal decompression. The latter event is widely developed throughout the HHC, and characterised by biotite–garnet–sillimanite–cordierite assemblages and migmatitic leucosomes produced by partial melting of metamorphic rocks. Miocene peraluminous leucogranitic magmas (Lombardo et al., 1993) are emplaced in the upper part of HHC (Black Gneiss and Rongbuck Formation), as large sheet-like intrusions (Nuptse and Makalu plutons) and dike swarms (Fig 1a).

Syn-metamorphic deformations gave rise to an E–W trending composite (*S*1/*S*2) foliation, that dips moderately towards the north or northeast with down-dip to slightly oblique mineral lineation. The composite foliation was subsequently folded with development of large-scale NE–SW trending upright antiforms and synforms (Fig. 1b).

2.1. Extensional faults and synkinematic dykes of the Imja Kola valley

In the Imja Khola valley, high grade orthogneiss and migmatitic gneiss of the Namche Migmatite Orthogneiss extensively crop out along the southern flank of the Taboche Antiform (Fig. 2). The metamorphic foliation dips moderately to gently towards the southeast and synkinematic mineral assemblages consist of feldspar, biotite, sillimanite, garnet ± cordierite. Moreover, the common occurrence of anatectic leucosomes has been interpreted as evidence of local partial melting in metamorphic rocks under high temperature–low pressure conditions (Pognante and Benna, 1993). Recently, Carosi et al. (1999) have reported the occurrence of a system of NE–SW trending extensional shear/fault zones injected by synkinematic leucogranitic dykes along the northern side of the Imja Kola valley (Fig. 2). The fault zones cross-cut the metamorphic foliation at very low angle and dip moderately to gently towards south and southeast, with southward plunging slickenside striations or stretching lineations (Fig. 2A). Kinematic indicators such as asymmetric structures within faults and the local occurrence of *S*–*C* fabrics, all indicate a southward-directed normal movement coupled with a component of dextral strike-slip shear (Carosi et al., 1999). The peraluminous leucogranites within the extensional shear zones, correspond to a system of dykes of variable size (decimetre to decametre width), which strike NE–SW, parallel to the shear zones, and dip moderately southeast. Most of the dykes have NE–SW striking foliations parallel to the shear zones, with south or southeast plunging mineral lineations outlined by alignment of biotite and tourmaline grains (Fig. 2A). In the larger dykes the foliation is preferentially developed in the outer portions, where the sigmoidal deflection of foliation planes between extensional shear planes also defines decimetre scale *S*–*C* structures with a top-to-southeast normal sense of shear. At the thin section scale the foliation is defined by the shape preferred orientation of magmatic biotite and tourmaline. This early magmatic fabric is locally overprinted by plastic deformation mainly defined by subgrain boundaries in quartz grains. The emplacement of dykes dated at 13.7 ± 0.3 Ma is slightly younger than the age of anatectic leucosomes in the host metamorphic rocks dated at 15.9 ± 0.2 Ma (Tonarini et al., 1994). According to Carosi et al. (1999), these age relations indicate that extensional faulting and dike emplacement were nearly coeval with late stage high temperature–low pressure metamorphism in the lower part of HHC.

The dykes, similar in composition and textures to the large leucogranitic intrusions and dike swarms in the overlying upper portion of HHC, have medium-grained predominantly equigranular textures. Constituent minerals are: quartz, K-feldspar, plagioclase, biotite ± white mica ± garnet, with zircon, apatite and tourmaline as accessory phases. Large perthitic K-feldspar and quartz grains are the main constituents with a minor amount of euhedral plagioclase and titanium-rich biotite. Plagioclase ranges in composition from andesine to oligoclase with albitic rims. Myrmekitic textures and graphic intergrowths of quartz and plagioclase are also common. White mica occurs as

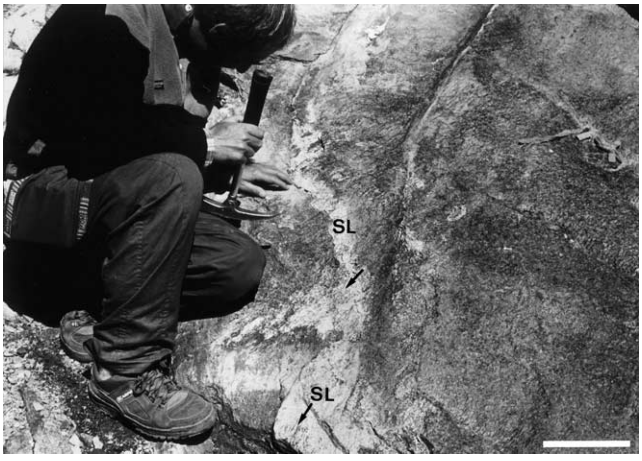

Fig. 3. Outcrop example of poorly foliated leucogranite dyke cross-cut by a sillimanite layer (SL), moderately dipping towards the south with moderately to gently plunging mineral lineations (small arrows). The layer is discontinuous and shows great variations in thickness. In the leucogranite the deformation is strongly partitioned into the portion cross-cut by the sillimanite layer (centre of photo). Scale bar: 20 cm.

euhedral grains on K-feldspar and biotite indicating a late magmatic crystallisation, while garnet occurs rarely as rounded subhedral grains associated with biotite. Euhedral grains of black tourmaline are often so abundant that they represent a distinctive feature of these intrusive bodies.

3. Sillimanite layers

3.1. General features

At the outcrop scale the most distinctive features of synextensional dykes in the fault zones are S-to-SE-dipping foliated layers and/or bands, which cross-cut the dike foliation at a low angle (Fig. 3). They are made up of fine-grained sillimanite grains or fibres with a strong preferred orientation defining a southward plunging lineation (Fig. 2B). Further, the congruous steps on the foliation plane give a top-to-the-south sense of shear, which is consistent with extensional faults movement. The sillimanite layers show variable length (decimetre to metre) and thickness (millimetre to centimetre) and have a heterogeneous distribution with discontinuous and anastomosing patterns.

On the basis of different sizes, morphologies and degree of development, the following types have been distinguished: (a) sillimanite-bearing fractures (type-1): thin discontinuous and irregularly spaced fractures and/or veinlets (Fig. 4a); (b) sillimanite folia (type-2): more continuous and regularly spaced layers with anastomosing patterns around deformed granitic pods (Fig. 4b); (c) sillimanite bands (type-3): well-foliated bands of centimetre width, which are made up of multiply interleaved, thick sillimanite foliae and intensely deformed granitic layers (Fig. 4c).

At the outcrop scale (Fig. 3) the most distinctive features of the sillimanite layers are the sharp contacts and straight boundaries with the leucogranite and the abrupt textural and compositional differences with respect to the leucogranite such as: (i) very fine grain size, and (ii) disappearance of magmatic minerals (mostly feldspar and biotite).

3.2. Microscopic features

Samples of granitic rocks (location in Fig. 2), have been collected in some synextensional dykes and examined in thin-section. Several thin-sections were cut with an orientation normal to the foliation and parallel or normal to the lineation defined by preferred orientation of sillimanite fibres or grains (i.e. the *XZ* and *YZ* planes of the finite strain ellipsoid). Some thin rock slices were also examined under scanning electron microscope to analyse the fracture system and relationships between sillimanite and magmatic texture.

At the thin-section scale, sillimanite layers are almost completely made up of fibrolite mats and/or prismatic sillimanite grains with a minor amount of fine-grained white mica, generally occurring along layer boundaries. Microcracks and/or thin fractures cross-cutting the layers at high angle are filled by aggregates of very fine-grained white mica and chlorite. Moreover, prismatic sillimanite is often affected by microboudinage with boudin necks filled by very fine-grained white mica. The layers are preferentially developed in the portion of dykes characterised by crystal–plastic deformation overprinting the earlier magmatic fabric (Fig. 5a). Large grains of igneous quartz show undulose extinction and subgrain boundaries. Irregular and/or interlobate subgrain boundaries and fine-grained quartz new grains with shape-preferred orientation indicate grain boundary migration and dynamic recrystallisation.

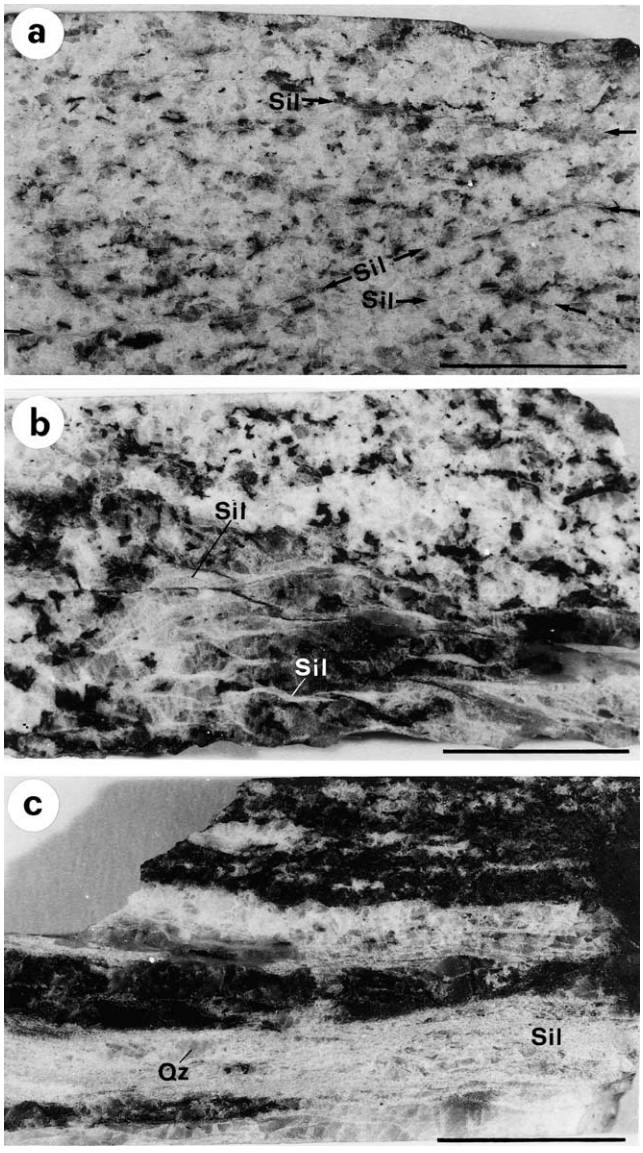

Fig. 4. Photographs of leucogranite samples with sillimanite layers (Sil). (a) Weakly deformed leucogranite with thin type-1 sillimanite-bearing fractures (black arrows). Scale bar: 1 cm. (b) Foliated leucogranite with anastomosing type-2 sillimanite foliae (lower half of the photo). Note the sharp boundaries between sillimanite layers and leucogranite. Scale bar: 1 cm. (c) Foliated leucogranite with type-3 sillimanite bands alternating with deformed granitic portions. Within the sillimanite layers, relict minerals such as quartz (Qz) are still preserved. Scale bar: 1 cm.

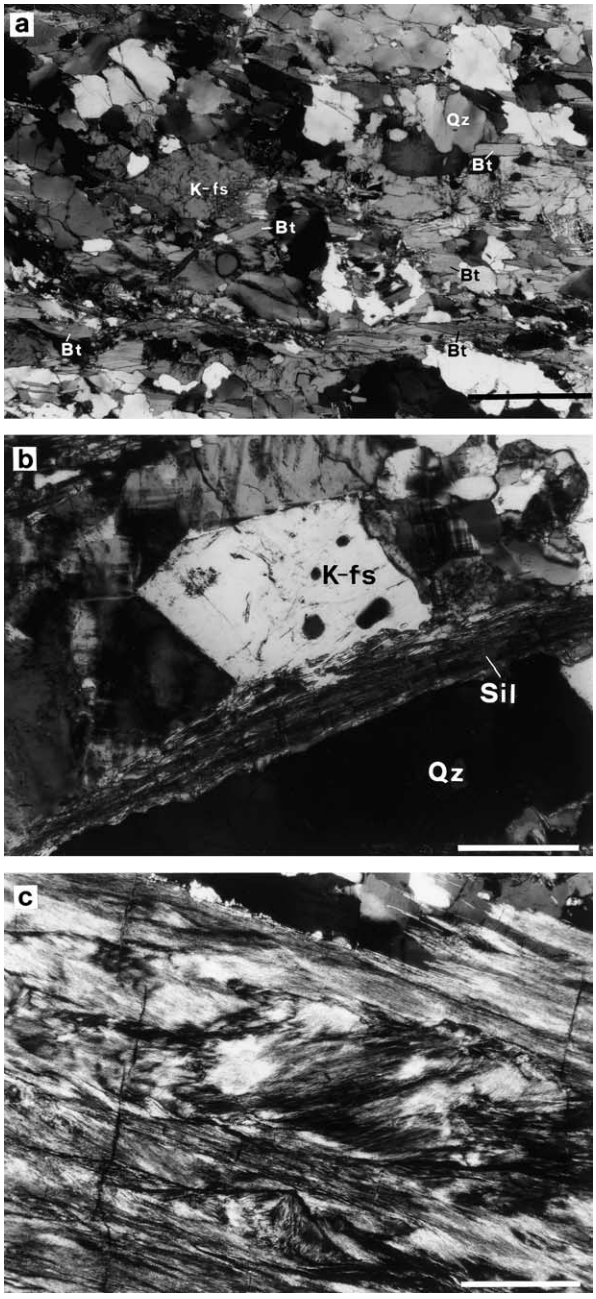

Fig. 5. Photomicrographs of textural features of sillimanite layers and relationships with leucogranite fabric. (Qz: quartz, K-fs: K-feldspar, Bt: biotite, Ms: muscovite, Sil: sillimanite). (a) leucogranite showing early magmatic fabric, mainly defined by shape-preferred orientation of biotite, overprinted by crystal–plastic deformation with development of subgrain domains. Crossed nicols, scale bar: 3 mm. (b) Sillimanite layer showing growth of sillimanite across grain boundaries and microcline domains in large deformed igneous feldspar (upper boundary of the layer). Crossed nicols, scale bar: 1 mm. (c) Detail of large fibrolite layer in which several fibrolite strands have different orientation and mutual cross-cutting relations. In the adjacent leucogranite fabric (upper right corner of the photo), fibrolite cross-cuts subgrain boundaries in fine-grained quartz newgrains. Crossed nicols. Scale bar: 0.2 mm.

K-feldspar shows undulose extinction, microcline domains and core-mantle textures consisting of a thin rim of fine grained quartz, albite and orthoclase new grains while biotite and plagioclase grains are weakly kinked. These strain features, namely grain boundary migration in quartz grains and marginal dynamic recrystallisation in feldspar indicate solid state deformation under high temperature condition (550–650 °C; Tribe and D'Lemos, 1996). Microstructural relations between sillimanite and host granite fabric observed along the layers boundaries, are characterised by the following features: (i) grain boundaries of igneous mineral are cross-cut at high angle by sillimanite grains and/or fibres without any deflection (Fig. 5b); (ii) twin boundaries in plagioclase as well as microcline domains and mantled rims in K-feldspar are not deflected where intersected by sillimanite; and (iii) fibrolite is concentrated along grain boundaries of igneous minerals, often showing radiating fibres that project into the grains at high angles.

All these indicate that sillimanite growth overprints magmatic minerals and both igneous and solid-state fabrics. Within the layers, prismatic sillimanite grains and fibrolite mats have a well-defined preferred orientation nearly parallel to the layer boundaries (Fig. 5b). Detailed observations reveal that: (i) most of the fibrolite mats are made up of multiple strands having different orientations and mutual cross-cutting relations, (ii) within strands, fibrolite needles are commonly deformed and affected by crenulation microfolds (Fig. 5c). Magmatic minerals (quartz, biotite, feldspar and tourmaline) occur as relic grains in the sillimanite layers, in which they exhibit strong grain-size reduction and shape variation compared with the grains in the magmatic fabric outside the layers. The three types of sillimanite layers show different textural and deformation features, which are described as follows.

3.2.1. Type-1—sillimanite-bearing fractures

These correspond to thin and discontinuous intergranular cracks filled by prismatic sillimanite or fibrolite and fine-grained white mica. They nucleate within deformed igneous minerals (K-feldspar and quartz) and/or in fine-grained recrystallised newgrains as mantled textures around large, strained, igneous K-feldspars. Intergranular cracks form a network of nearly parallel and intersecting fractures with development of fractured zones and/or microfault zones, in which cataclasis is testified by the occurrence of small angular grains split off by tensile cracks (Fig. 6a). The majority of fractures are nearly planar or slightly curvilinear; however en échelon segments (Fig. 6b) and secondary tensile cracks linking fractures give rise to development of pull-apart zones filled by sillimanite grains and fine-grained white mica (Fig. 6a and b). The increase in fracture density and their coalescence led to the local development of irregularly spaced veinlets having planar or curvilinear shapes (Fig. 6c), straight contact with igneous minerals and abrupt variation in width (0.2–0.7 mm in thickness). These

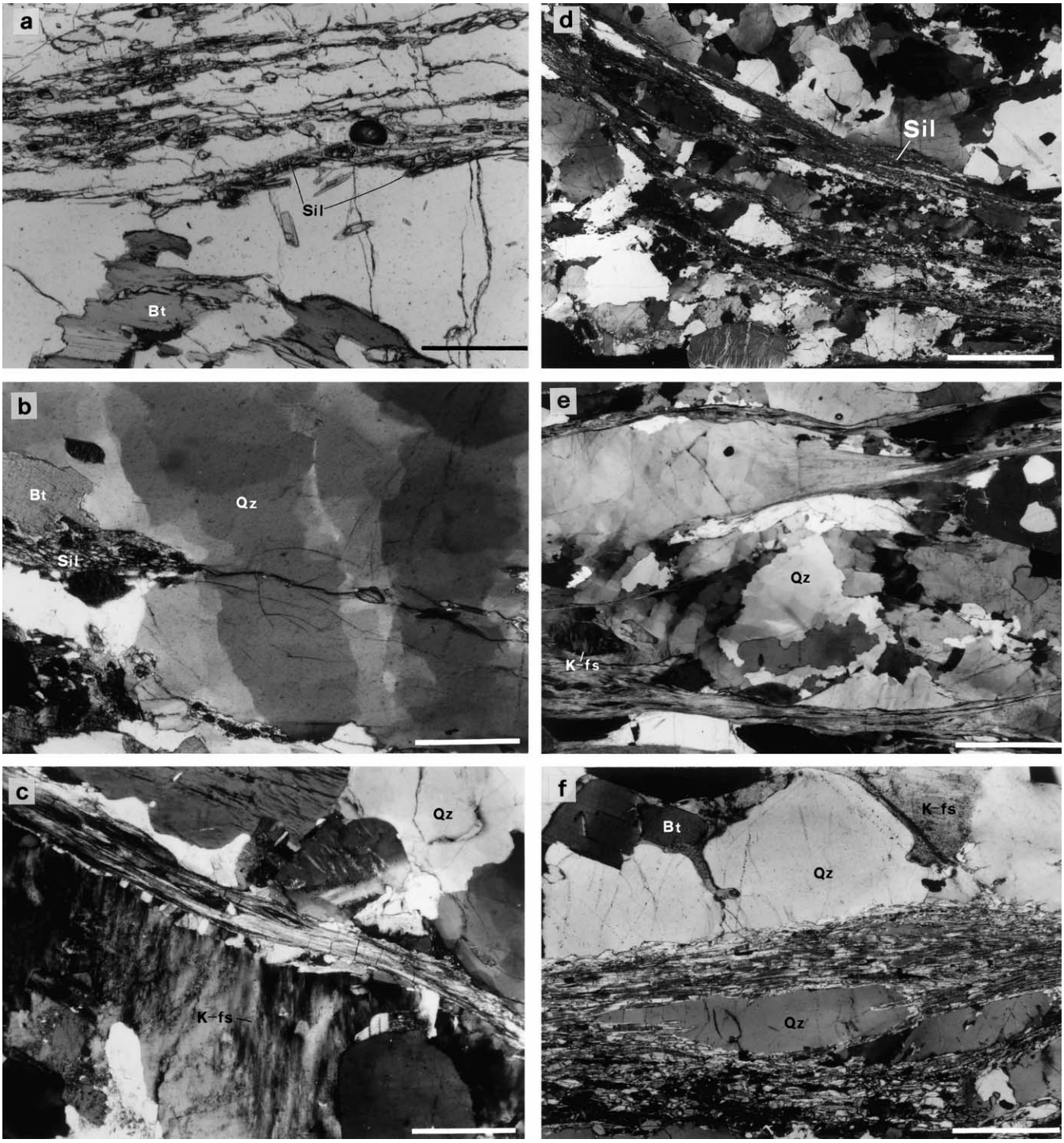

Fig. 6. Photomicrographs of type-1 sillimanite-bearing fractures and type-2 sillimanite foliae. (a) Intergranular fractures cross-cutting igneous grains and filled by fine-grained phyllosilicates and sillimanite. Secondary tensile cracks linking fractures lead to cataclasis of grains and development of dilational jogs or voids (centre of photo) filled by sillimanite. Plane polarised light, scale bar: 1 mm. (b) Detail of fracture cross-cutting large deformed igneous grain. Fracture consists of en échelon segments and terminates in a void filled by sillimanite grains. Crossed nicols, scale bar: 1 mm. (c) Thin sillimanite-bearing veinlet, which cross-cuts igneous fabric and mantled rim around large deformed feldspar. Crossed nicols, scale bar: 3 mm. (d) Type-2 sillimanite foliae highlighting the textural differences between igneous fabric and sillimanite layers. The latter show sharp contacts with leucogranite and the growth of sillimanite overprints the pre-existing magmatic texture. Igneous minerals are affected by edge resorption along sillimanite layer boundaries and the anastomosing pattern of foliae define some interfolia domains (centre of the photo). Crossed nicols, scale bar: 3 mm. (e) Interfolia domains wrapped by thin fibrolite folia. Within the domains igneous fabric and crystal–plastic deformation are preserved. Along the boundaries with fibrolite foliae the minerals show intense resorption of their edges in contact with fibrolite. Crossed nicols, scale bar: 2 mm. (f) Detailed view of the boundary between sillimanite folia and interfolial domain. The edge resorption of mineral in contact with sillimanite strongly contrasts with the igneous texture preserved in the domains (upper half of the photo) where sillimanite grains or fibres are lacking. Elongated grains within sillimanite folia represent intrafolia domains. Crossed nicols, scale bar: 1 mm.

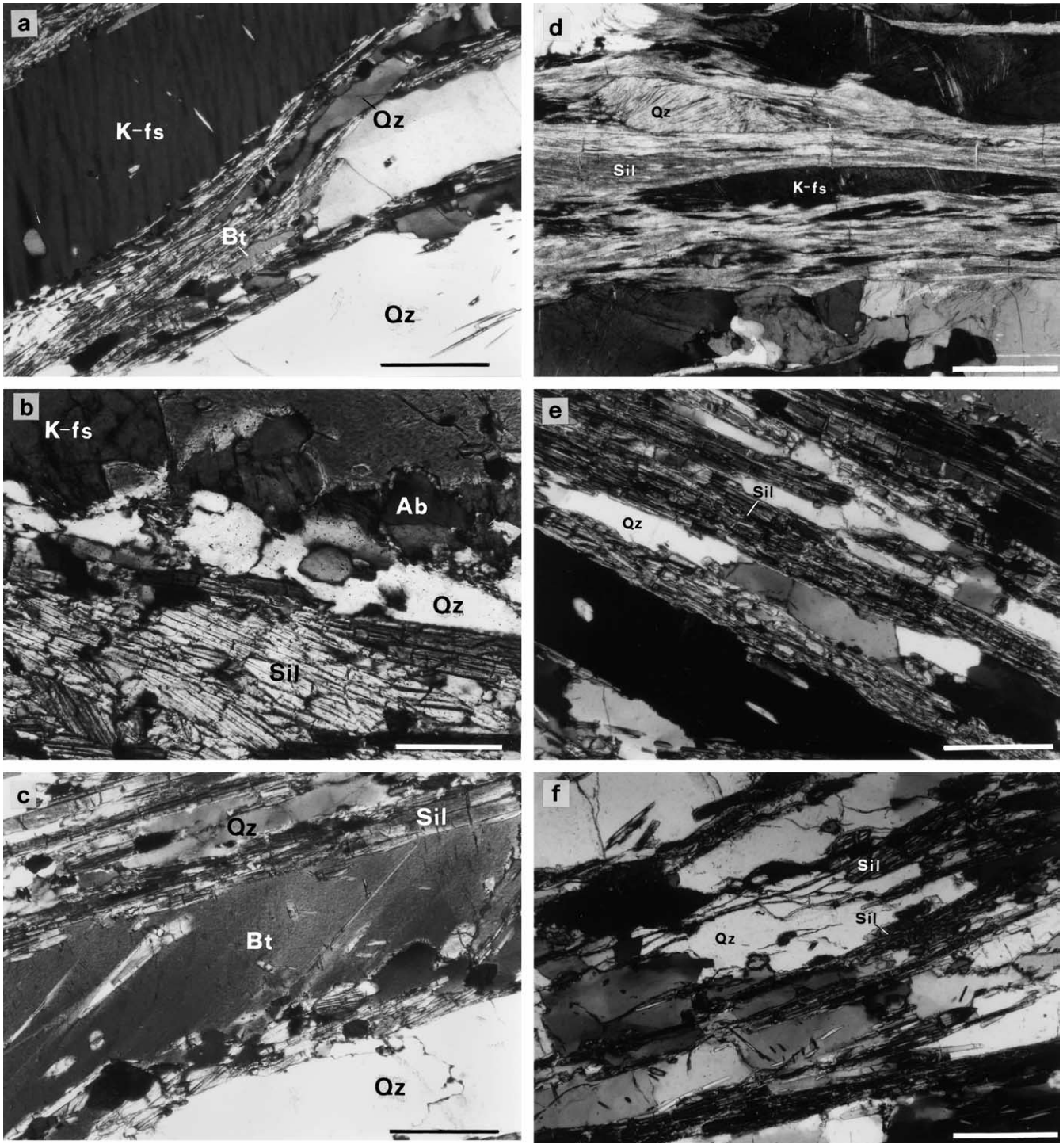

Fig. 7. (a) Detail of strongly resorbed K-feldspar (K-fs) with perthitic lamellae truncated by sillimanite grains. Crossed nicols, scale bar: 2.5 mm. (b) Prismatic sillimanite growing on a pre-existing mantled texture made up of quartz and albite new grains around a large K-feldspar. Crossed nicols, scale bar: 1 mm. (c) Growth of sillimanite along resorbed edges of magmatic biotite and within it as isolated grains. Crossed nicols, scale bar: 2.5 mm. (d) Intrafolia domains represented by lenticular quartz and feldspar grains wrapped and cross-cut by sillimanite fibres. Crossed nicols, scale bar: 1 mm. (e) Intrafolia domains represented by aggregates of quartz grains with elongated shapes and straight boundaries in contact with sillimanite Crossed nicols, scale bar: 1 mm. (f) Fracture network at the termination of large sillimanite folia showing the fracture control on the development of elongated grains. Crossed nicols, scale bar: 2 mm.

veinlets are filled by fibrolite mats with a minor amount of fine-grained white mica, generally occurring along the veinlet boundaries. Fibres show a preferred orientation parallel to the veinlet boundaries (Fig. 6c); however, several fibrolite strands with different orientations and affected by crenulating microfolds occur in the internal portion of the larger veinlets. The igneous minerals along the veinlets typically exhibit a moderate resorption of their edges in contact with sillimanite (Fig. 6c).

3.2.2. Type-2—sillimanite foliae

These form networks of sub-parallel and anastomosing layers (Fig. 6d), that are more planar and wider (0.5–1.5 mm) than the type-1 fractures or veinlets, and are further characterised by significant compositional and textural variations with respect to the host leucogranite. These include: (i) preferred orientation of mineral grains, (ii) low modal content of igneous grains, quartz, feldspar and biotite, and (iii) intense resorption of magmatic minerals within the layers, which attain a fine grain-size and lenticular shapes. The foliae are made up of both fibrolitic and prismatic sillimanite with a minor amount of very fine-grained white mica and chlorite, which fill tensional fractures cross-cutting the layers at high angle. Within the foliae, strong preferred orientation of sillimanite fibres or grains defines a foliation parallel to the layer boundaries, which almost completely overprints any previous texture or fabric (Fig. 6d). Some kinematic features such as: (i) asymmetric microfolds, (ii) fibrolite strands having an oblique orientation with respect to layer boundaries, and (iii) thin fibrolite foliae that curve into the layers, indicate a top-to-south sense of shear. Sillimanite foliae often terminate in fractured zones of millimetre width, defined by nearly parallel thin fractures, which show the same geometry and morphology of the above described type-1 fractures. Relic portions of leucogranite fabric in the type-2 sillimanite foliae correspond to interfolia and intrafolia domains. Interfolia domains are represented by subrounded or lenticular millimetre to centimetre sized granitic pods wrapped by sillimanite foliae (Fig. 6e). Within them the original igneous fabric and mineral assemblages are almost completely preserved. Igneous grains maintain their original medium-grained size and euhedral–subhedral shapes. Further, they show crystal plastic deformation with development of undulose extinction, subgrain domains and lobate grain boundaries. In these domains the most significant textural variations occur along the contacts with the sillimanite foliae, where the igneous grains exhibit straight boundaries and a strong resorption of their edges in contact with sillimanite. Evidence for grain resorption is easily recognisable in feldspars and biotite; the former show truncation of perthitic lamellae and/or mantled textures by sillimanite fibres or grains (Fig. 7a and b). In biotite grains, the (001) cleavage planes are truncated by sillimanite (Fig. 7c). Although intense resorption of igneous minerals is restricted to their boundaries in contact with sillimanite foliae,

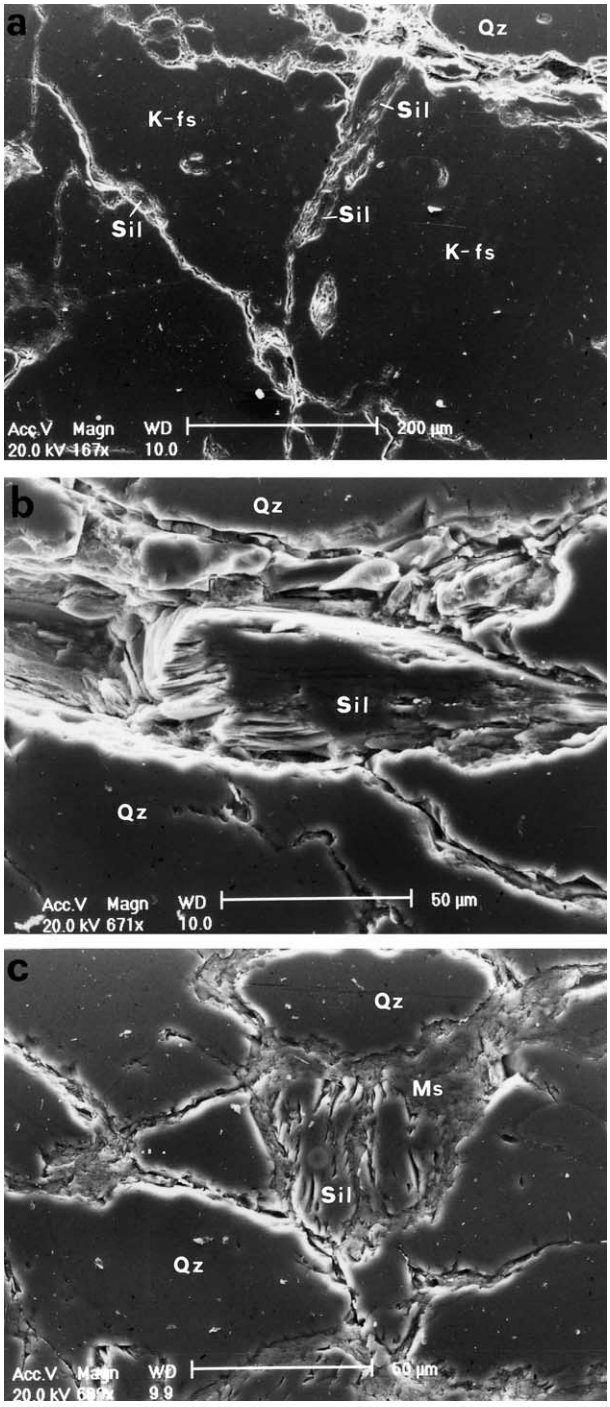

Fig. 8. Scanning electron microscope photographs of polished sections. (Qz: quartz, K-fs: K-feldspar, Ms: muscovite, Sil: sillimanite). (a) Intergranular cracks within quartz and feldspar grains along a sillimanite layer boundary. Some sillimanite grains occur within the cracks. (b) Detail of a crack within a quartz grain, filled by sillimanite. (c) Cracks filled by randomly oriented muscovite produced by later alteration of sillimanite.

detailed optical and SEM observations reveal the occurrence within the interfolia domains of thin intergranular and transgranular fractures, which emanate from the sillimanite layer. These fractures cross-cut the igneous grains and lead to the development of cataclastic textures

Table 1
Mean aspect ratio of quartz grains in the *XZ* and *YZ* sections measured in undeformed leucogranite granite and in intrafolia domain within sillimanite layers (50 grains measured for each thin section)

	Intrafolia domains				Igneous fabric			
Sample	95-3	95-4	95-9	95-24	95-3	95-4	95-9	95-24
R_{XZm}	7.7	10.5	10.2	9.6	1.7	1.4	1.3	1.2
R_{YZm}	3.1	3.3	3.4	2.9	1.5	1.4	1.2	1.2

consisting of fine-grained angular fragments bounded by fractures or microcracks (Fig. 8a), which are filled by sillimanite and fine grained muscovite (Fig. 8b and c). Intrafolia domains consist of deformed quartz and more rarely feldspar and/or biotite minerals, which can occur either as aggregates of a few grains or as single grains, both wrapped by sillimanite (Fig. 6f). In the intrafolia grains, crystal–plastic deformation (undulose extinction and subgrain boundaries) pre-date sillimanite growth as shown by sillimanite grains or fibres that truncate or cross-cut subgrain boundaries (Fig. 7d and e). The most prominent textural features of the intrafolia domains are: (i) the fine grain size, and (ii) the elongated and/or lenticular shapes of relic igneous grains (Fig. 7d and e). Grain shape variation of minerals in the intrafolia domains with respect to the igneous fabric was analysed by measuring the aspect ratios of quartz grains on *XZ* and *YZ* sections (parallel and orthogonal to the lineation defined by sillimanite fibres). As shown in Table 1 and Fig. 9 (*XZ* section), quartz grains in the igneous fabric have almost homogeneous and low mean aspect ratios ($1 < R_{XZ} < 2.5$), which strongly increase ($R_{XZ} > 9$) in the intrafolia domains within the sillimanite layers. The shape variation of igneous grains in these domains seems partly due to grain resorption as testified by lenticular shapes (Fig. 7d). However, most of the grains have elongated shapes with straight boundaries in contact with sillimanite characterised by a limited amount of grain resorption (Fig. 7e). These features are indicative that in the intrafolia domains, both grain size reduction and shape variation were mainly controlled by earlier brittle fracturing of larger igneous grains, as recognisable at the end of sillimanite folia, which terminate in a system of fractures (Fig. 7f).

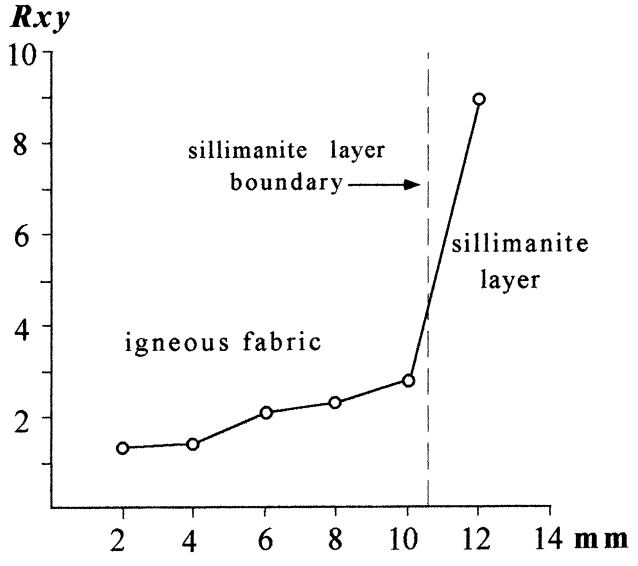

Fig. 9. Diagram illustrating the variation of mean aspect ratio of quartz grains on distance (in millimetres) from igneous fabric to intrafolia domains within sillimanite layer (*XZ* section). Measurements of aspect ratio were performed on thin sections along cross-sections normal to leucogranite–sillimanite layer boundary.

3.2.3. Type-3—sillimanite bands

These structures of centimetre to decimetre width, are made up of alternating sillimanite-rich and granitic layers with development of well-foliated fabrics (Fig. 4c). Sillimanite-rich layers mostly consist of prismatic sillimanite grains, showing an increase in grain-size and a well-preferred orientation, which defines the foliation within these bands. Fibrolitic sillimanite rarely occurs and it is mainly concentrated along layer boundaries as aggregates of radiating fibres, cross-cutting grain boundaries of igneous minerals at high angle. Intrafolia domains occur

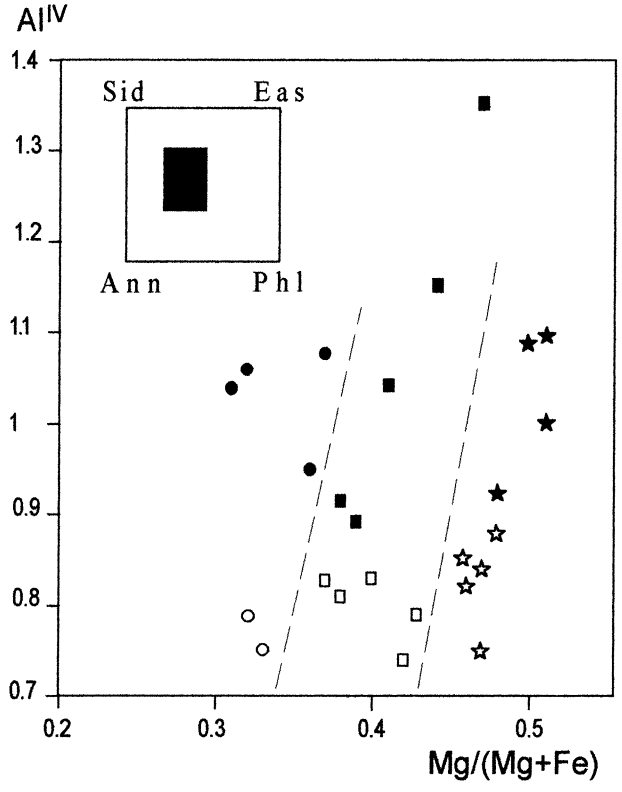

Fig. 10. Variation of biotite composition as a function of sillimanite replacement. Open symbols: unfibrolitised magmatic biotite in the leucogranite; closed symbols: fibrolitised biotites within or along sillimanite layers; circle: sample 95-9; square: sample 95-25; star: sample 95-4. In the insert is shown the position of figure with respect to the biotite end-member composition (Sid: siderite; Eas: eastonite; Ann: annite; Phl: phlogopite).

Table 2
Microprobe analyses of fibrolitised and unfibrolitised biotite. $Mg_v = Mg/(Mg + Fe)\%$ 95-4: P1 biotite core in granitic portion, P2 fibrolitised biotite rim, P6 small biotite in sillimanite layer; 95-9: P16 biotite core in granitic portion, P18 fibrolitised biotite rim, P23 fibrolitised biotite rim; 95-25: P23 biotite in granitic portion, P12 biotite core in sillimanite layer, P13 biotite rim in sillimanite layer, P16 fibrolitised biotite in sillimanite layer

Wt%	95-4			95-9			95-25			
	P 1	P 3	P 6	P 16	P18	P 23	P 3	P 12	P 13	P 16
SiO_2	35.29	37.09	34.88	34.87	34.79	34.39	35.23	35.63	36.17	36.59
Al_2O_3	19.87	20.24	21.04	19.13	19.8	20.53	19.37	19.47	20.66	21.96
TiO_2	3.22	1.53	1.48	3.49	2.01	2.23	3.4	3.34	2.78	1.63
FeO	18.89	17.76	17.38	23.18	21.74	20.32	21.23	20.01	19.78	16.77
MnO	0.12	0.09	0.1	0.23	0.24	0.28	0.34	0.17	0.19	0.14
MgO	9.17	10.56	9.99	6.41	7.04	6.69	6.94	7.3	7.56	8.44
CaO	0	0.01	0	0.02	0.02	0.0	0	0.02	0.01	0.02
Na_2O	0.19	0.05	0.06	0.09	0.16	0.11	0.22	0.26	0.08	0.1
K_2O	9.56	9.14	8.93	9.69	9.75	9.61	9.9	9.76	9.7	8.95
Sum	96.31	96.52	93.81	97.14	95.57	94.22	96.65	96	96.97	94.63
Cation proportion on the basis of 22 oxygens										
Si	5.30	5.48	5.31	5.32	5.36	5.33	5.36	5.41	5.40	5.48
Al^{IV}	2.70	2.52	2.69	2.68	2.64	2.67	2.65	2.59	2.60	2.53
Al^{VI}	0.82	1.01	1.09	0.76	0.95	1.09	0.83	0.89	1.04	1.35
Ti	0.36	0.17	0.17	0.40	0.23	0.26	0.39	0.38	0.31	0.18
Fe	2.37	2.20	2.21	2.96	2.80	2.64	2.70	2.54	2.47	2.10
Mn	0.02	0.01	0.01	0.03	0.03	0.04	0.04	0.02	0.02	0.02
Mg	2.05	2.33	2.27	1.46	1.62	1.55	1.57	1.65	1.68	1.88
Ca	0.00	0.00	0.00	0.00	0.00	0.00	0.00	0.00	0.00	0.00
Na	0.06	0.01	0.02	0.03	0.05	0.03	0.07	0.08	0.02	0.03
K	1.83	1.72	1.74	1.89	1.92	1.90	1.92	1.89	1.85	1.71
Mg_v	0.46	0.51	0.51	0.33	0.37	0.37	0.37	0.39	0.41	0.47

more rarely than in the type-2 sillimanite folia and are made up of fine-grained elongated quartz, feldspar and biotite grains parallel to the sillimanite orientation. The granitic portions correspond to planar layers of millimetre to centimetre width, where the igneous fabric is preserved. Similarly to interfolia domains in the type-2 sillimanite foliae, they are characterised by fibrolitisation and grain boundary resorption of the minerals in contact with sillimanite layers. However, within them, thin sillimanite folia also occurs within inter and/or transgranular fractures, which are similar to the type-1 veinlets.

3.3. Mineral chemistry

The effects of grain resorption on the composition of fibrolitised K-feldspar and biotite have been investigated by microprobe analyses performed using a JEOL JXA 8600 microprobe (accelerating voltage 15 kV, beam current 10 nA, and beam diameter of 2 μm). K-feldspars affected by resorption do not show any variation in composition between unfibrolitised cores and the fibrolitised rims. Conversely biotites show abrupt compositional variation where affected by sillimanite growth. The compositions of biotite from texturally distinct sites in three samples, are given in Fig. 10 and Table 2. Biotites unaffected by sillimanite growth have uniform compositions from core to rim, while those in contact with sillimanite have rims enriched in octahedral Al and in phlogopite component with respect to their cores, which have a similar composition to the unfibrolitised biotites. The observed zonation in the fibrolitised biotites is due to increases in Al and Mg content and depletion in Ti, Fe and Na at the rims. The small relic grains of biotite within sillimanite layers have even more pronounced compositional variations, marked by strong increases in Al and Mg, decreased Ti and Fe, and the highest values of octahedral Al and phlogopite component (Table 2). Moreover, the growth of magnetite as small grains (50 μm) in association with sillimanite along the rims of fibrolitised biotite, is consistent with depletion of Fe and Ti from biotite. Biotites from the three samples analysed have different initial igneous compositions in terms of annite content; however, all show the same trends in composition where affected by sillimanite growth (Fig. 10).

4. Discussion

4.1. Origin of sillimanite

The leucogranitic dykes of the Imja Kola Valley are peraluminous melts belonging to the Miocene magmatism of the Himalayan belt. In the examined rocks, however, the occurrence of sillimanite as grains and/or fibres within fractures or layers and its growth overprinting magmatic fabrics reveal that sillimanite is not a product of direct magmatic crystallisation.

Several workers have proposed an origin for sillimanite overprinting earlier metamorphic and/or igneous fabrics by metasomatic processes due to base-cation leaching of pre-existing silicates (Vernon, 1979; Kerrick, 1987; Wintsch and Andrews, 1988). Some proposed sillimanite-forming reactions are given in Table 3. Vernon (1979), in particular, appealed to hydrogen metasomatism for fibrolisation of biotite, muscovite and feldspar in the Cooma Complex, Australia, (reactions [1]–[3] in Table 3). Kerrick (1987) explained the fibrolisation of biotite in the contact aureole of Donegal intrusion by circulation of acidic fluids enriched in HCl, released by intrusive bodies during a late stage of crystallisation (reaction [4] in Table 3). A slightly different mechanism has been suggested by Wintsch and Andrews (1988) for sillimanite growth as a replacement product of K-feldspar and biotite in a granitic pegmatite. They proposed a model of deformation-induced fibrolitisation with a metasomatic origin of sillimanite along micro-scale shear zones (reactions [5,6] in Table 3). In order to explain the absence of quartz and potassium-bearing minerals as product phases in association with sillimanite, they hypothesised a system open to all non-volatile chemical components.

In the examined example, microstructural and textural aspects such as: (i) the growth of sillimanite along feldspar and biotite margins, (ii) the compositional zoning of fibrolitised biotites, (iii) the occurrence of rare igneous minerals in the sillimanite layers as relic grains, and (iv) the low modal content of quartz within the layers, are all features that suggest a metasomatic origin of sillimanite/fibrolite by replacement of K-feldspar, biotite and albitic plagioclase following the reactions reported in Table 3. This could imply the circulation of acidic fluids not buffered by rock composition; moreover, the resorption and modal reduction of quartz grains within the sillimanite layers can be explained by the increased solubility of quartz in acidic fluids. The above reported reactions produce SiO_2, alkalis and H_2O (reactions [1], [3] and [5]), magnetite, Mg and Fe (reactions [2], [4] and [6]) in addition to sillimanite (Table 3). Fine-grained muscovite in association with sillimanite in the type-1 fractures and veinlets and the occurrence of small magnetite grains in association with sillimanite along the rims of fibrolitised biotite, could represent local sinks for K and Fe released from decomposition of orthoclase and biotite. However, the absence of new muscovite and quartz grains in the type-2 foliae and type-3 sillimanite bands seems to indicate that, in contrast to type-1 fractures, these layers represent small-scale (millimetre to centimetre size) systems open to fluid circulation and removal of some products of reactions.

4.2. Model of nucleation and development of shear bands

The replacement reactions of feldspar and biotite, reported in Table 3, may be driven by several factors such as: (i) temperature and /or compositional differences between dykes and host rocks, (ii) pressure variation, and (iii) applied deformation (Wintsch and Andrews, 1988). In the study area, significant temperature gradients between leucogranite dykes and host gneiss are considered unlikely because leucogranitic dykes were emplaced in the high-grade gneissic rocks when metamorphic rocks where still at high temperatures, as testified by the similar cooling ages of anatectic leucosomes and leucogranitic dykes (Carosi et al., 1999). Moreover, the similar mineralogy of the dykes and host gneissic rocks suggests that the development of chemical gradients that may have driven sillimanite-producing reactions is also unlikely. A variation in pressure, particularly a decompression, might favour the development of sillimanite in the presence of an intragranular fluid. However, under such circumstances, the sillimanite crystallises as unoriented fibres at grain boundaries rather than

Table 3
Sillimanite forming reactions

$2\underset{\text{K-feldspar}}{KAlSi_3O_8} + 2H^+ = \underset{\text{sillimanite}}{Al_2SiO_5} + 5SiO_2 + H_2O + 2K^+$	[1] (Vernon, 1979)
$2\underset{\text{biotite}}{K(Mg,Fe)_3AlSi_3O_{10}(OH)_2} + 14H^+ = \underset{\text{sillimanite}}{Al_2SiO_5} + 5SiO_2 + 2K^+ + 6(Mg,Fe)_2 + 9H_2O$	[2] (Vernon, 1979)
$2\underset{\text{albite}}{NaAlSi_3O_8} + 2H^+ = \underset{\text{sillimanite}}{Al_2SiO_5} + 5SiO_2 + H_2O + 2Na^+$	[3] Vernon, 1979)
$2\underset{\text{biotite}}{K(Mg_xFe_{1-x})3AlSi_3O_{10}(OH)_2} + 14HCl = \underset{\text{sillimanite}}{Al_2SiO_5} + 5SiO_2 + 2KCl + 6(Mg_xFe_{1-x})Cl_2 + 9H_2O$	[4] (Kerrick, 1987)
$2\underset{\text{K-feldspar}}{K_{0.8}Na_{0.2}AlSi_3O_8} + 2H^+ = \underset{\text{sillimanite}}{Al_2SiO_5} + 5SiO_2(aq.) + 1.6K^+ + 0.4Na^+ + H_2O$	[5] (Wintsch and Andrews, 1988)
$2\underset{\text{biotite}}{K_2(Fe_{1.8}Mg_{3.0}Al_{1.0})Si_{5.4}Al_{2.6}O_20(OH_{3.2}F_{0.8})} + 6H^+ = 1.8\underset{\text{sillimanite}}{Al_2SiO_5} + 0.6\underset{\text{magnetite}}{Fe_3O_4} + 3.6SiO_2(aq.) + 2K^+ + 3.0Mg^{++} + 0.8F^- + 1.2e^- + 4.6H_2O$	[6] (Wintsch and Andrews, 1988)

within narrow layers with a well-preferred orientation, unless decompression accompanied by deformation. The microstructural aspects of sillimanite layers, namely: (i) preferred orientation of sillimanite fibres or grains, (ii) occurrence in the fibrolite mats of multiple strands with different orientation and truncations between them, and (iii) crenulated or tightly folded fibrolite strands, are all features that imply non-hydrostatic stress during sillimanite growth. Particularly, as stated by Vernon (1987), these features are evidence for high non-coaxial strains within the sillimanite layers compared with the rock outside of the layers. Therefore, deformation is interpreted as a major factor in driving biotite and feldspar replacement reactions within the syntectonic dykes of the Imja Kola valley. Pressure solution due to differential stresses along grain boundaries is an effective mechanism for driving replacement reactions in retrograde shear zones. However, this mechanism may also be effective under high temperature conditions (Wintsch and Andrews, 1988). Indeed, any increase in (i) internal energy of mineral grains due to stored strain (elastic strain and plastic strain associated with lattice defects) or (ii) surface energy due to grain size reduction, affects the stability of minerals and enhances their solubility in a fluid phase. In the sillimanite layers, the growth of new minerals that have different compositions to the host igneous grains indicate that incongruent pressure solution was the dominant mechanism of sillimanite growth. This implies the development of chemical gradients away from the sites of dissolution located along the edges of igneous feldspar and biotite grains and the removal of alkalis and silica by an intergranular fluid phase.

In order to attempt a model for the nucleation and growth of sillimanite-layers in the granitic dykes, the following features must be considered: (i) geometric, structural and kinematic features of the sillimanite layers are consistent with their development during large scale extensional faulting. Their orientation and top-to-the-south sense of shear suggest they form synthetic shear planes with respect to the major extensional faults; (ii) the common occurrence of sharp and straight boundaries between sillimanite layers and host leucogranite indicates that deformation was localised along pre-existing planar structures such as fracture zones; (iii) nucleation of sillimanite layers corresponds to development of intergranular fractures (type-1 fractures) in which a circulating fluid phase interacted with the leucogranite; (iv) after development of sillimanite veinlets and foliae, microstructural features indicate that these layers become zones of high non-coaxial strain with respect to the rock outside of the layers; and (v) the growth and stability of sillimanite within fractures and layers indicate amphibolite facies conditions. The pressure and temperature conditions during sillimanite growth can be indirectly estimated by metamorphic conditions in the host rock. Indeed, cooling of leucogranite dykes was coeval with Late Himalayan low pressure/high temperature metamorphism in the host gneissic rocks. This could imply pressure and temperature conditions of 2–4 kbar and 600 °C (Pognante and Benna, 1993) during the formation of sillimanite layers.

All the above-mentioned features indicate the sillimanite layers represent amphibolite facies small-scale shear zones, whose nucleation and growth was a function of deformation and fluid distribution. An evolutionary model can be outlined as follows (Fig. 11):

1. At the early stage, (type-1 sillimanite-bearing fractures), localised brittle deformation is responsible for the development of intergranular fractures, which nucleate as synthetic shear fractures (R and P shears; Sylvester, 1988), that ultimately evolved into through-going microfault zones. These zones are characterised by cataclasis, grain-size reduction of igneous grains and increased permeability with respect to the bulk rock, as a consequence of grain-scale dilatancy. Therefore, they can act as efficient pathways for circulation of acidic fluids, which interact with igneous minerals to give new 'softer' sillimanite and white mica assemblages as a product of feldspar and biotite replacement. Particularly, the higher surface energies and solubility of fractured grains (compared with the larger unfractured grains outside of the fault zones), strongly promoted replacement reactions, via incongruent pressure solution.
2. The lengthening and linking up of fractures by stepover segments, as a consequence of shear displacement, led to the development of dilational jogs (Sibson, 1985) in which sillimanite can grow extensively (Fig. 11a). These processes were responsible for the early development of sillimanite-bearing veinlets, where the preferred orientation of sillimanite grain and/or fibres is parallel or slightly oblique to the veinlet boundaries, suggesting a dilational opening parallel to the shear planes (Fig. 11a). The geometry of the early formed sillimanite-veinlets is comparable with the type-D veins described by McCaig (1987), with extension parallel to the shear planes.
3. The progressive widening and linking up of the early formed veinlets, which accommodated the displacement between shear fractures, led to the development of more continuous and wider type-2 sillimanite foliae, that represent available pathways for channelised fluid circulation (Fig. 11b). This allowed a more intense replacement of igneous minerals, as testified by strong resorption of feldspar and biotite, with removal of alkalis and silica and concomitant crystallisation of sillimanite. The ability of sillimanite to accommodate large strain by grain boundary sliding (fibre-sliding; Vernon, 1987) compared with the other minerals, particularly feldspars, results in a softening in the sillimanite foliae. Therefore these layers represent weaker zones with respect to surrounding granite, in which strain was partitioned via reaction softening (e.g. White and Knipe, 1978). In these foliae, the lenticular/elongated shapes of quartz and feldspar

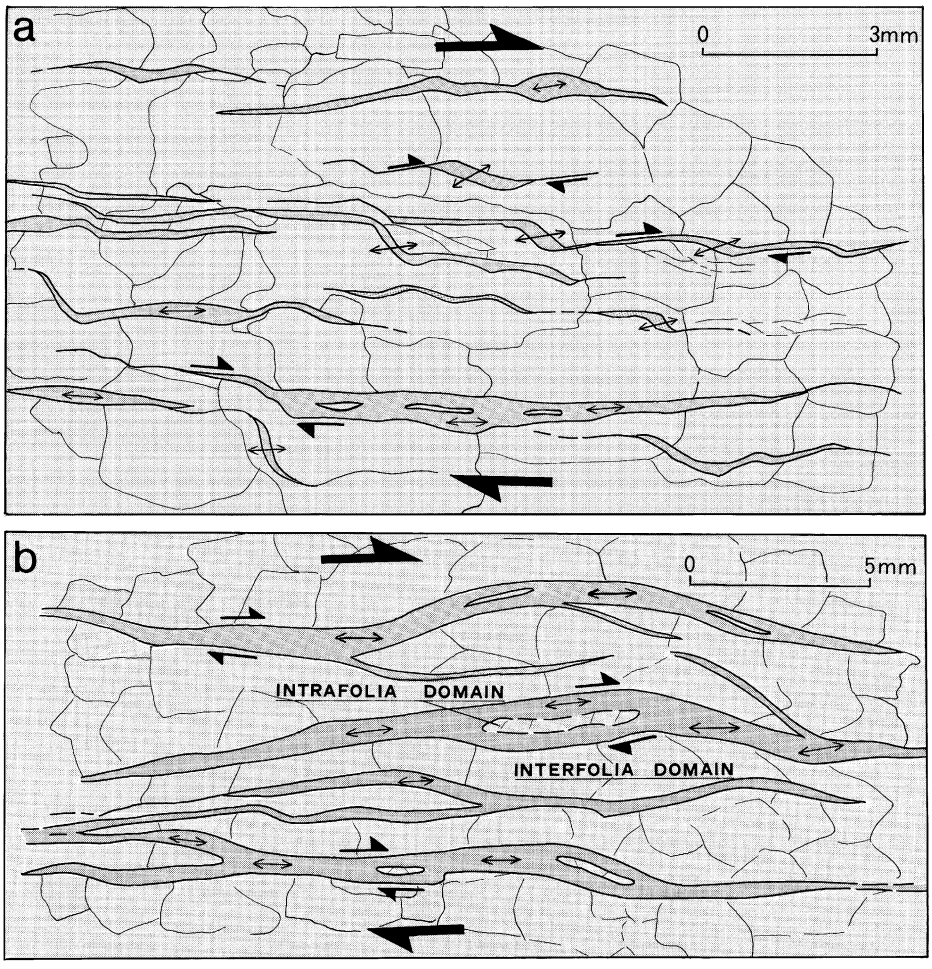

Fig. 11. Scheme of nucleation and evolution of sillimanite shear bands (grey shaded area) within leucogranite (light shaded area). Large half black arrows: bulk sense of shear; small half black arrows: sense of shear along fractures; thin double arrows: preferred orientation of sillimanite grains and fibres. (a) Development of sillimanite-bearing fractures and veinlets (type-1) as a result of fluid circulation within microfault zones. Dilational jogs develop between stepover segments linking fractures. Within them the orientation of sillimanite indicate extension parallel to the shear planes. (b) Growth of sillimanite folia (type-2) by coalescence of early formed veinlets. Anastomosing patterns of sillimanite folia lead to development of granitic pods (interfolial domains) in which igneous texture is preserved, while igneous minerals in contact with sillimanite show strong resorption of their edges. Some small elongated grains occur within the folia as intrafolia domains.

grains (intrafolia domains; Fig. 11b), although partly related to solution of their edges in contact with sillimanite, mainly reflect the earlier brittle fracturing of larger igneous grains. The type-3 bands represent the final product of fluid influx, replacement reactions and strain partitioning within sillimanite foliae, which at this stage behave in a similar manner to mica-rich phyllonitic layers in low grade shear zones.

The sequence of events describing the development of sillimanite-bearing shear zones indicates a transition from brittle to plastic deformation and underlines the role of fractures in allowing permeability for fluid circulation. In particular, the limitation of fluid interaction to the fractured zones, without any diffusion in the adjacent rocks, indicates that fluid flow was channelised within a fractured open system (Oliver, 1996), in which deformation, fluid flow and metamorphic reactions operate together in the development of ductile shear zones. Further, during the evolution of these shear zones from the early type-1 fractures to the final type-3 bands, the strain remains localised within these narrow zones rather than being distributed through the rock. This is shown at the hand sample and outcrop scale by heterogeneous development of sillimanite shear zones and in particular, by the absence of shear deformation in the adjacent leucogranitic rocks.

4.3. Role of pre-existing weak zones

In the proposed model, nucleation of sillimanite layers was driven by localisation of shear fractures, that in the Coulomb–Griffith failure theory occur at angles of about 30° to σ_1 in isotropic material. In a normal fault environment, where σ_1 can be assumed subvertical, the moderate to gentle dip of sillimanite shear bands (30–50°) does not match the Coulomb–Griffith failure criterion and suggests

they formed at high angles (>40°) to σ_1. In anisotropic rocks, Donath (1961) and Hobbs et al. (1976) demonstrated that existing planes of weakness, with lower cohesion than in the bulk rock, allow the development of shear fractures parallel to the weak planes and at higher angles to σ_1. Moreover, brittle failure can occur by either increasing σ_1, decreasing σ_3 or lowering effective stress, until the Mohr circle intersects the failure envelope for planes of weakness (Hobbs et al., 1976, fig. 7.35). Brittle shear zones, developed in rocks with a pre-existing foliation, often have a system of shear planes with similar orientation to the pre-existing foliation (Passchier, 1984). In the examined case, the near parallelism of sillimanite layers with magmatic foliation and, in particular, the nucleation of sillimanite-bearing shear fractures on domains of ductile deformation (strained igneous grains and/or intergranular regions of subgrains and newgrains), means that pre-existing weaknesses controlled the orientation of early fractures (type-1 sillimanite-bearing fracture).

4.4. Processes controlling fracture development

Retrograde shear zones with *S–C* fabrics, homogeneously developed throughout the whole rock or restricted to discontinuous shear bands (Lister and Snoke, 1984; Gapais, 1992) are distinctive features of syntectonic granites. Greenschist facies shear zones are mostly initiated by brittle fracturing, which localises subsequent ductile deformation (Segall and Pollard, 1983; Segall and Simpson, 1986; Gibson, 1990; Tourigny and Tremblay, 1997). In such shear zones, fluids are thought to be important, driving both the development of dilatant fractures and chemical reactions that lead to the formation of new 'softer' mineral assemblages. In this example fluids contribute to the development of brittle-fracturing by reducing effective stress. However, as development of the sillimanite shear bands is restricted to pre-existing zones of plastic strain, these are interpreted to have played a main role in driving nucleation of shear fractures. Crystal–plastic processes can lead to high densities of dislocation tangles and/or twins within grains, which restrict further ductile deformation and induce work-hardening (Knipe, 1989). Moreover, (i) different rates of deformation between adjacent grains and (ii) the diffusive concentration of point defects or vacancies along grain boundaries, may promote brittle fracture along the grain boundaries. These processes are responsible for fracture development and/or sub-critical crack growth (Atkinson, 1984), leading to failure under a wide range of conditions. The resultant increase in void density and/or the occurrence of cracks allows the local infiltration of a fluid phase, which may drive further strain localisation in two main ways: (i) mechanical: high fluid pressure reduces effective stress and induces hydraulic fracturing; (ii) chemical: corrosion and reaction at crack tips promote fracture propagation (stress corrosion).

Work hardening leading to brittle failure mainly occurs during low temperature crystal plastic deformation dominated by dislocation glide along slip planes (Knipe 1989). In the granitic rocks, deformation is strongly controlled by the mechanical behaviour of feldspar. The brittle–plastic transition (i.e. from cataclastic flow to dislocation creep) in feldspars occurs over a wide range of conditions from greenschist to amphibolite grade and it is complete at about upper amphibolite grade (Tullis and Yund, 1987). Furthermore, the presence of a fluid phase is also important because, at high fluid pressures, brittle deformation and crack growth also occur at high temperature (Tullis and Yund, 1987). Therefore, the nucleation of discontinuous shear zones within leucogranite dykes of the Imja Khola valley was most likely caused by the combined effects of earlier strain localisation and fluid interaction. Localised deformation by plastic processes such as dislocation creep (Kirby, 1985) and/or strain localisation, resulting from stress concentrations between grains with different material properties (e.g. difference in grain size), promoted work hardening and the local development of distributed microcracks. These in turn allowed fluid infiltration, promoting crack propagation, mineral transformation (replacement reactions) and partitioning of ductile deformation into weaker layers.

5. Conclusions

The leucogranitic dykes of the Imja Khola valley were emplaced within top-to-the-south extensional shear zones during late-Himalayan high temperature/low pressure metamorphism. Deformation outlasted emplacement and during syn-tectonic cooling, strain partitioning coupled with fluid interaction gave rise to sillimanite-bearing shear bands. The development of these structures within narrow dykes emplaced within the extensional shear zones and containing kinematic indicators consistent with top-to-the-south extension, indicate a direct relation between sillimanite-bearing shear zones and fault activity. This example illustrates that development of heterogeneous shear bands, even under amphibolitic facies conditions, can be strongly favoured by: (i) work hardening, which leads to brittle fracturing, and (ii) fluid interactions. The development of cracks and fractures might be envisaged as a sequence of short-lived brittle events that punctuate a more prolonged history of plastic deformation. Such a behaviour is favoured by repeated conditions of fluid overpressure, which lead to embrittlment in a similar fashion to melt-filled fractures in migmatitic regions (e.g. Davidson et al., 1994). Further, variation in grain size and the occurrence of mechanical anisotropies exert a strong influence on controlling the orientation of shear bands. The development of brittle–ductile shear zones under amphibolite facies conditions can lead to the syndeformational growth of 'weak' minerals, such as fibrolitic sillimanite, which behave similarly to phyllosilicates in lower grade shear zones.

Acknowledgements

The author is very grateful to R. Scott and A. McCaig for careful reviews and suggestions and to R.J. Norris for comments and editorial assistance. G. Vagelli and R. Albani are also thanked for assistance during microprobe and SEM analyses. Fieldwork was financially supported by CNR (Everest-K2 project and CSGSDA—Pisa).

References

Atkinson, B.K., 1984. Subcritical crack growth in geological materials. Journal Geophysical Research 89, 4298–4312.

Beach, A., 1979. Pressure solution as a metamorphic processes in deformed terrigeneous sedimentary rocks. Lithos 12, 51–58.

Bell, T.H., Cuff, C., 1989. Dissolution, solution transfer, diffusion versus fluid flow and volume loss during deformation/metamorphism. Journal Metamorphic Geology 7, 425–447.

Bordet, P., 1977. Géologie de la dalle du Tibet (Himalaya central). Mémoires hors série de la Societé géologique de France 8, 235–250.

Brodie, K.H., Rutter E.H., 1985. On the relationships between deformation and metamorphism, with special reference to the behaviour of basic rocks. In: Thompson A.B., Rubie D.C. (Eds.), Metamorphic Reactions, Kinetics, Texture and Deformation. Advances in Physical Geochemistry 4, pp. 138–179.

Brunel, M., 1983. Étude pétro-structural des chevauchements ductiles en Himalaya (Népal oriental et Himalaya du Nord-Ouest). Thése Doct. ès Sciences, Université de Paris VII.

Burchfiel, B.C., Chen, Z., Hodges, K.V., Liu, Y., Royden, L.H., Changrong, D., Xu, L., 1992. The South Tibetan Detachment System, Himalayan orogen: extension contemporaneous with and parallel to shortening in a collisional mountain belt. Geological Society of America Special Paper 269.

Burg, J.P., Brunel, M., Gapais, D., Chen, G.M., Kiu, G.H., 1984. Deformation of leucogranites of the crystalline main central thrust sheet in southern Tibet (China). Journal of Structural Geology 6, 535–542.

Carosi, R., Musumeci, G., Pertusati, P.C., 1999. Extensional tectonics in the Higher Himalayan Crystallines of Khumbu Himal, Eastern Nepal. In: Macfarlane A., Sorkhabi R., Quade J. (Eds.), Himalaya and Tibet: Mountains Roots to Mountains Tops. Geological Society of America Special Paper 328, pp. 211–223.

Carosi, R., Lombardo, B., Molli, G., Musumeci, G., Pertusati, P.C., 1998. The South Tibetan Detachment System in the Rongbuk valley, Everest Region: deformation features and geological implications. Journal of Asian Earth Science 16, 299–311.

Davidson, C., Schmid, S.M., Hollister, L.S., 1994. Role of melt during deformation in the deep crust. Terra Nova 6, 133–142.

Donath, F.A., 1961. Experimental study of shear failure in anisotropic rocks. Geological Society of American Bulletin 72, 985–990.

Gapais, D., 1992. Shear structures within deformed granites: mechanical and thermal indicators. Geology 17, 1144–1147.

Gibson, R.G., 1990. Nucleation and growth of retrograde shear zones: an example from the Needle Mountains, Colorado, USA. Journal of Structural Geology 12, 339–350.

Hobbs, B.E., Means, W.D., Williams, P.F., 1976. An Outline of Structural Geology. John Wiley & Sons, New York.

Kerrick, D.M., 1987. Fibrolite in contact aureoles of Donegal, Ireland. American Mineralogist 72, 240–254.

Kirby, S.H., 1985. Rock mechanics observations pertinent to the rheology of the continental lithosphere and the localisation of strain along shear zones. Tectonophysics 119, 1–27.

Knipe, R.J., 1989. Deformation mechanism–recognition from natural tectonites. Journal of Structural Geology 11, 127–146.

Lister, G.S., Snoke, A.W., 1984. *S–C* mylonites. Journal of Structural Geology 6, 617–638.

Lombardo, B., Pertusati, P.C., Borghi, S., 1993. Geology and tectonomagmatic evolution of the eastern Himalaya along Chomolungma–Makalu transect. In: Treloar, P.J., Searle, M.P. (Eds.), Himalayan Tectonics. Geological Society of London Special Publication 74, pp. 341–355.

McCaig, A.M., 1987. Deformation and fluid–rock interaction in metasomatic dilatant shear bands. Tectonophysics 135, 121–132.

Oliver, N.H.S., 1996. Review and classification of structural controls on fluid flow during regional metamorphism. Journal Metamorphic Geology 14, 477–492.

Passchier, C.W., 1984. The generation of ductile and brittle shear bands in a low-angle mylonite zone. Journal of Structural Geology 6, 273–281.

Pognante, U., Benna, P., 1993. Metamorphic zonation, migmatization and leucogranites along the Everest transect of Eastern Nepal and Tibet: record of an exhumation history. In: Treloar, P.J., Searle, M.P. (Eds.), Himalayan Tectonics. Geological Society of London Special Publication 74, pp. 328–340.

Segall, P., Pollard, D.D., 1983. Nucleation and growth of strike-slip faults in granite. Journal of Geophysical Research 88, 555–568.

Segall, P., Simpson, C., 1986. Nucleation of ductile shear zones on dilatant fractures. Geology 14, 56–59.

Sibson, R.H., 1985. Stopping of earthquake ruptures at dilational fault jogs. Nature 316, 248–251.

Sylvester, A.G., 1988. Strike-slip faults. Geological Society of America Bulletin 100, 1666–1703.

Tonarini, S., Lombardo, B., Ferrara, G., Marcassa, P., 1994. Partial melting in the Namche Migmatite of Khumbu Himal (Nepal Himalaya). Mineralogica Petrografica Acta 37, 277–294.

Tourigny, G., Tremblay, A., 1997. Origin and incremental evolution of brittle/ductile shear zones in granitic rocks: natural examples from the southern Abitibi Belt, Canada. Journal of Structural Geology 19, 15–27.

Tribe, I.R., D'Lemos, R.S., 1996. Significance of hiatus in down-temperature fabric development within syn-tectonic quartz diorite complexes, Channel Islands, UK. Journal of Geological Society of London 153, 127–138.

Tullis, J., Yund, R.A., 1987. Transition from cataclastic flow to dislocation creep of feldspar: mechanism and microstructures. Geology 15, 606–609.

Vernon, R.H., 1979. Formation of late sillimanite by hydrogen metasomatism (base-leaching) in some high grade gneisses. Lithos 12, 143–152.

Vernon, R.H., 1987. Growth and concentration of fibrous sillimanite related to heterogeneous deformation in K-feldspar–sillimanite metapelites. Journal Metamorphic Geology 5, 51–68.

White, S.H., Knipe, R.J., 1978. Transformation and reaction enhanced ductility in rocks. Journal of Geological Society of London 135, 513–516.

Wintsch, R.P., 1985. The possible effects of deformation on chemical processes in metamorphic fault zones. In: Thompson, A.B., Rubie, D.C. (Eds.), Metamorphic Reactions, Kinetics, Texture and Deformation. Advances in Physical Geochemistry 4, pp. 251–268.

Wintsch, R.P., Andrews, M.S., 1988. Deformation induced growth of sillimanite "stress" mineral revisited. Journal of Geology 96, 143–161.